9-3-2021

Comparative Safety Analysis of Accelerator Driven Subcritical Systems and Critical Nuclear Energy Systems

Run Luo

Shripad Revankar

Fuyu Zhao

Article

Comparative Safety Analysis of Accelerator Driven Subcritical Systems and Critical Nuclear Energy Systems

Run Luo [1,*], Shripad T. Revankar [2] and Fuyu Zhao [3]

1   School of Resource & Environment and Safety Engineering, Cooperative Innovation Center for Nuclear Fuel Cycle Technology and Equipment, University of South China, Hengyang 421001, China
2   School of Nuclear Engineering, Purdue University, West Lafayette, IN 47907, USA; shripad@purdue.edu
3   School of Nuclear Science and Technology, Xi'an Jiaotong University, Xi'an 710049, China; fuyuzhaoxjtu@163.com
*   Correspondence: luorun@usc.edu.cn

Abstract: The accelerator driven subcritical system (ADS) has been chosen as one of the best candidates for Generation IV nuclear energy systems which could not only produce clean energy but also incinerate nuclear waste. The transient characteristics and operation principles of ADS are significantly different from those of the critical nuclear energy system (CNES). In this work, the safety characteristics of ADS are analyzed and compared with CNES by a developed neutronics and thermal-hydraulics coupled code named ARTAP. Three typical accidents are carried out in both ADS and CNES, including reactivity insertion, loss of flow, and loss of heat sink. The comparison results show that the power and the temperatures of fuel, cladding, and coolant of the CNES reactor are much higher than those of the ADS reactor during the reactivity insertion accident, which means ADS has a better safety advantage than CNES. However, due to the subcriticality of the ADS core and its low sensitivity to negative reactivity feedback, the simulation results indicate that the inherent safety characteristics of CNES are better than those of ADS under loss of flow accident, and the protection system of ADS would be quickly activated to achieve an emergency shutdown after the accident occurs. For the loss of heat sink, it is found that the peak temperatures of the cladding in the ADS and CNES reactors are lower than the safety limit, which imply these two reactors have good safety performance against loss of heat sink accidents.

Keywords: accelerator driven subcritical system; critical reactor; safety analysis; accident

1. Introduction

Nuclear energy plays a key role in the development of clean energy and reduction of carbon emissions all over the world. The accelerator driven subcritical system (ADS) is a new nuclear energy system which could not only produce clean energy but also incinerate actinide nuclides and long-lived radioactive fission products [1]. The ADS device consists of a subcritical core, a high-energy proton accelerator and a neutron spallation target, in which the fission process is sustained by a spallation neutron source. Compared with critical nuclear energy systems (CNESs), ADSs have a better performance concerning nuclear waste transmutation due to a harder neutron spectrum. In recent years, ADS has been attracting more and more attention because of its superior neutronics and safety characteristics [2]. Conceptual designs of three types of experimental accelerator driven systems (XADSs) have been studied by the European Atomic Energy Community within its fifth framework program [3], which includes a zero-power subcritical facility YALINA, an 80 MW lead bismuth eutectic (LBE) cooled XADS, and a 50 MW multi-purpose hybrid research reactor MYRRHA for high-tech applications. A roadmap for developing Accelerator Transmutation of Waste (ATW) technology was presented by the United States Department of Energy (DOE) [4]; several researchers studied the physics design for using sodium or LBE as coolant of the ATW systems [5,6]. The Japan Atomic Energy Agency (JAEA) has

investigated an 800 MW LBE-cooled subcritical reactor with a 1.5 GeV proton accelerator to transmute minor actinides [7]. Research on a hybrid power extraction reactor (HYPER) was carried out by the Korea Atomic Energy Research Institute (KAERI) to produce energy and transmute nuclear waste [8]. The China lead-based reactor (CLEAR) and the Chinese initiative accelerator driven subcritical system (CiADS) have been proposed by the Chinese Academy of Sciences for the transmutation of nuclear waste and sustainability of nuclear energy development [9,10]. The conceptual design of a 10 MW LBE-cooled CLEAR has been completed, and a proton accelerator with 650 MHz multicell superconducting radio frequency (SRF) in the CiADS device and an accelerator-driven advanced nuclear energy system (ADANES) have been proposed [11].

The component of the ADS system and its operation principle are significantly different from those of the CNES system. To ensure safe operation and optimize reactor design of the ADS system, it is necessary to investigate its transient characteristics under accident conditions and analyze its advantages and disadvantages compared to the CNES system. Several codes have been developed for safety analysis of ADS by using a neutronics model coupled with thermal and hydraulic feedback effects [12]. Reference Chen et al. [13] analyzed some safety characteristics for a lead-bismuth eutectic (LBE) cooled ADS using the extended SIMMER-III code. In addition, Suzuki et al. [14] investigeted the unprotected blockage in a single fuel assembly and severe core-melt accidents with the updated SIMMER-III. The neutronics and thermal-hydraulics coupled simulation program was developed by the FDS team for the design and research of lead or LBE cooled ADS reactors [15], and three typical transient accidents were simulated with NTC code, such as beam trip and transient overpower condition [16]. Reference Lu et al. [17] used the RELAP5 program for a safety analysis on loss of flow accidents and external source transients of an 800 MW ADS with the code modifications of the point-kinetics model and the thermal property package. These studies are mainly focused on the transient characteristics of ADS itself, but did not analyze the differences of inherent safety features between ADS and CNES. Reference Schikorr [18] has built a lumped parameter model of the neutronics and thermal-hydraulics to demostrate the differences of dynamic behavior between ADS and critical fast reactor. The transient calculations of critical and subcritical LBE-cooled reactors were carried out by using the FAST code [19], including the dynamic behaviors of overpower, loss of flow and loss of coolant accidents. Reference Wang et al. [20] simulated the loss of heat sink accident for both ADS and the critical reactor by NTC code, in which the amplitude equations of core neutronics are the point-kinetics model. However, the point-kinetics method may be inaccurate in the case of severe source perturbations involving strong reactivity feedback that produce great flux distortion, which may happen during a serious accident [21,22]. Therefore, the variation of the spatial shape function with time should be considered in the ADS model. In this work, a space–time neutron diffusion model of the ADS reactor is developed to replace the point-kinetics neutron model to meet the requirement of satisfactory accuracy for transient safety analysis. The differential equations of neutron diffusion are calculated by the spatial discretization with the finite difference method and the time discretization with a backward differentiation formula (BDF) method [23,24]. In addition, the space distribution of the spallation neutron source in the diffusion model is calculated by the Monte Carlo method. The safety characteristics of ADS are analyzed under typical accident conditions and its advantages and disadvantages are compared to the CNES system.

The objective of this research is to analyze differences of the safety characteristics of the LBE-cooled ADS and CNES by using a neutronics and thermal-hydraulics coupled simulation code named ARTAP. The developed code consists of a space–time neutron diffusion equation with a spallation neutron source model and a thermal-hydraulics model with a package of thermophysical properties, which could be used for calculations of both the LBE-cooled ADS and the LBE-cooled CNES. Three typical accidents are calculated by ARTAP code, including reactivity insertion, loss of flow, and loss of heat sink. In addition, the accident simulations are not only performed in the case of unprotected transient,

but also in the case of protected transient, i.e., transient with interruption of accelerator beam for ADS and with insertion of shutdown rod for CNES. The transient behavior of the reactor power and the temperatures of the fuel, cladding, and coolant are investigated during the accident sequences.

2. Calculation Model and Method

In this work, the Italian 80 MW LBE-cooled reactor is chosen as the research object to study differences of the safety characteristics of the ADS and CNES [19]. On the one hand, we adopt this reactor because it is sufficiently representative for the various ADS conceptual designs [25]. On the other hand, compared with other ADS conceptual types we can obtain the detailed composition and geometric distribution of all materials (fuel, cladding, coolant, spallation target, reflector, control rod, etc.) for this reactor through the existing literature and technical reports. After obtaining these basic data and empirical correlation, the calculation of spallation neutron distribution between the accelerator proton beam and the metal target, the processing of macroscopic cross sections in the reactor core, and the use of material thermophysical properties for the thermal-hydraulics analysis could be carried out during the reactor modeling process.

The ADS device consists of a subcritical core, a high-energy proton accelerator and a heavy metal spallation target. The CNES reactor is a critical core; its operational process is implemented by the control rods. The configuration of the LBE-cooled ADS and CENS is shown in Figure 1. It can be seen from Figure 1a that the accelerator proton beam is introduced into the target and then hits the metal target to initiate the spallation reaction. As a result of the spallation reaction process, neutrons will be supplied to the subcritical reactor core, which serves as an external neutron source to maintain fission chain reactions. On the one hand, the power level could be changed by adjusting the beam intensity during the transient operating conditions. On the other hand, the external neutron source in the core could be interrupted by quickly cutting off the accelerator beam so as to achieve emergency shutdown protection under accident conditions. The heat produced in the core will be carried out by the coolant of lead bismuth eutectic (LBE). In the heat exchanger (IHX), the coolant of the primary side is high temperature LBE, and the coolant of the secondary side is an organic diathermic fluid. As shown in Figure 1b, the CNES core itself could sustain a chain fission reaction without external neutron source, and the power level could be adjusted by the control rods during the transient process. The secondary circuit of CNES is similar to that of ADS.
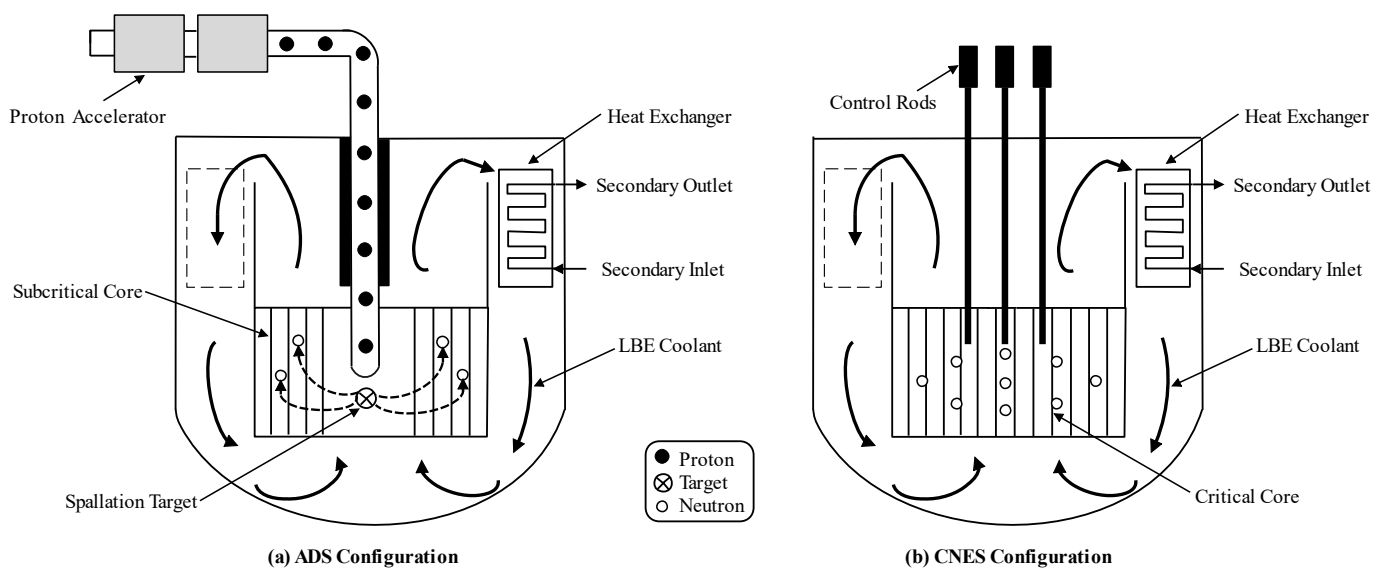

Figure 1. Configuration of the LBE-cooled ADS and CNES.

2.1. Process of Numerical Calculation

In this paper, a developed ARTAP code is applied in comparative analysis of the safety characteristics between the LBE-cooled ADS and CNES, which is comprised of a steady-state analysis module and a transient analysis module. The steady-state analysis module couples a one-dimensional neutron diffusion equation and a thermal-hydraulics single-channel model [26]. The single channel model includes the heat conduction in the fuel element and the heat transfer from cladding to coolant. A flowchart of the neutronics and thermal-hydraulics coupled calculation is shown in Figure 2.
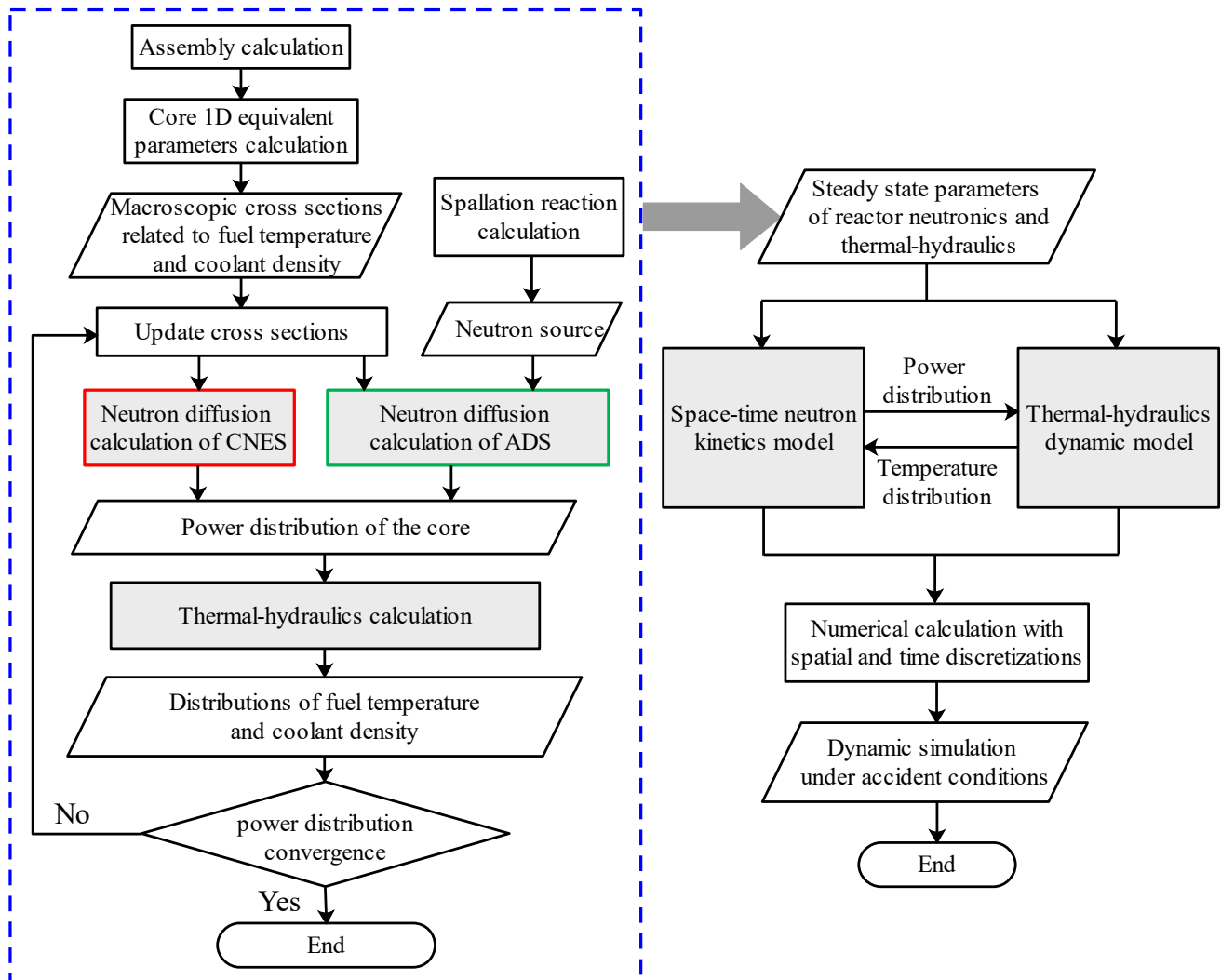

Figure 2. Numerical calculation flowchart.

Before the assembly calculation starts, the geometric arrangement and detailed composition of all materials (fuel, cladding, coolant, spallation target, reflector, control rod, etc.) for the ADS and CNES reactors need to be determined through the existing literature and technical reports. After obtaining these basic data and empirical correlation, the calculation of neutron source distribution in the ADS spallation target, the processing of macroscopic cross sections for the subcritical core of ADS and the critical core of CNES, and material thermophysical properties introduced into the thermal-hydraulics model of both reactors could be carried out during the process of simulation calculation and comparative analysis, as shown in Figure 2. When macroscopic cross sections and spallation neutron source are obtained, steady-state neutron diffusion equations of these two reactors could be solved, respectively, by the power iteration method. According to the power distribution by the

neutronics calculation, the thermal-hydraulics analysis is performed for both reactors, and the obtained distributions of fuel temperature and coolant density are selected as the feedback parameters to update their nuclear cross sections. Then the neutron diffusion calculations are carried out for both reactors, respectively, to update the power distributions again. This coupling iterative process continues until some criterion for convergence is met. The steady-state parameters of reactor neutronics and thermal-hydraulics are provided as initial parameters for dynamic simulation. The numerical calculation of dynamic models is divided into two steps, i.e., the spatial discretization with the finite difference method and the numerical solution of nonlinear time-dependent differential equations with a backward differentiation formula (BDF) method [23].

2.2. Space–Time Neutron Diffusion Model

While the three-dimensional full core multi-physics modeling of nuclear reactor is an effective way to obtain the key information of the reactor core with high precision, the required data storage space is very huge and the running time is quite long. In a few special calculations like performing the reactor control system design, transient safety analysis or load following study, the detailed radial information of the reactor core is not necessarily needed due to the radially symmetrical layout of fuel assemblies and control rod banks [27]. Thus, a one-dimensional neutron diffusion model in the axial direction will be more preferable when the calculation precision is not reduced.

2.2.1. Space-Time Neutron Kinetics Model

The space and time dependent neutron kinetics model of the ADS reactor is as follows:

$$\frac{1}{v_a}\frac{\partial \phi(z,t)}{\partial t} = D\nabla^2\phi(z,t) - \Sigma_a\phi(z,t) + (1-\beta)\nu\Sigma_f\phi(z,t) + \sum_{j=1}^{6}\lambda_j C_j(z,t) + S(z,t) \quad (1)$$

$$\frac{\partial C_j(z,t)}{\partial t} = \beta_j\nu\Sigma_f\phi(z,t) - \lambda_j C_j(z,t); \quad j = 1,2,\ldots,6 \quad (2)$$

where v_a is the average speed of neutrons, ϕ is the neutron flux, z is the axial position, t is the time, D is the diffusion coefficient, Σ_a and Σ_f are the macroscopic cross section of absorption and fission, respectively, ν is neutrons yield per fission, S is the spallation neutron source, β is the total delayed neutron fraction, β_j is the delayed neutron fraction of group j, and C_j and λ_j are the delayed neutron precursor concentration and decay constant, respectively.

For the CNES reactor, the Equation (1) can be modified as:

$$\frac{1}{v_a}\frac{\partial \phi(z,t)}{\partial t} = D\nabla^2\phi(z,t) - \Sigma_a\phi(z,t) + (1-\beta)\nu\Sigma_f\phi(z,t) + \sum_{j=1}^{6}\lambda_j C_j(z,t) \quad (3)$$

The difference between Equations (1) and (3) is not only the absence of the source term in the critical core, but also the values of the cross-section parameters in Equations (1) and (3), which could be determined according to the composition and geometric distribution of all materials in the ADS and CNES cores. In the process of the neutron flux calculation, the finite difference method will be used for the discretization in space. This discretization is shown in Figure 3, and the size of each node is Δ_i. The power iteration method is used to calculate the steady-state diffusion equation [28], and the corresponding distribution of neutron flux could be determined by this iterative scheme. After the spatial discretization, neutron kinetics models could be transformed into the normal forms of time-dependent differential equations which could be solved by a backward differentiation formula (BDF) method with a scheme of implicit time discretization.
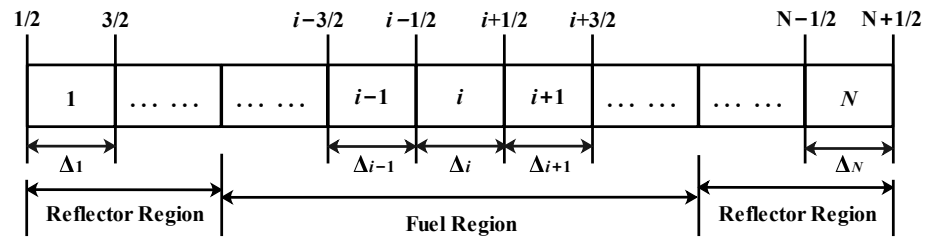
Figure 3. Spatial discretization in the axial direction.

2.2.2. Spallation Neutron Source Calculation

The space and energy distributions of the spallation neutrons $S(z, t)$ in the target for the ADS reactor are calculated by the Monte Carlo transport code, which could simulate the interaction between an accelerator proton beam and a metal target [29]. The beam footprint at the target is circular with a diameter of 0.16 m, and its height is 0.9 m. According to the geometric arrangement and material composition of the spallation target, a three-dimensional model of the target was built using the Monte Carlo code and the neutrons tracked in the spallation target were tallied into an output file, then the distribution of spallation neutrons could be obtained, which are used asa shape function of the spallation source during the process of ADS neutron diffusion calculation. The distributions of spallation neutrons along the axial direction of the core and its energy spectrum are shown in Figure 4.
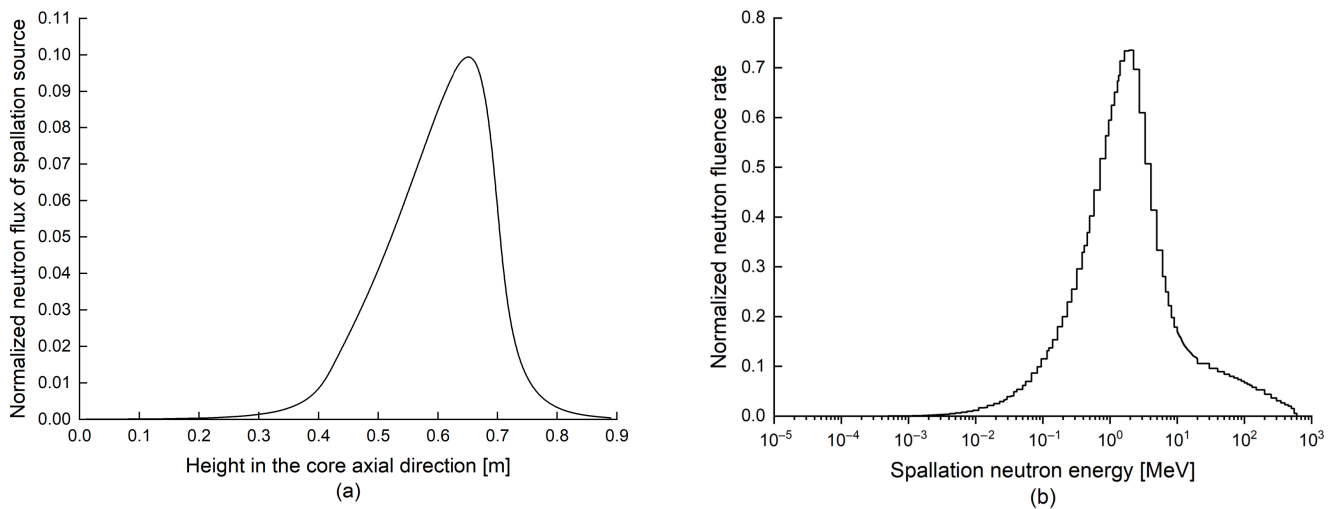

Figure 4. Space and energy distributions of the spallation neutron in the target.

In the process of transient simulation, the space and time-dependent spallation source term $S(z, t)$ in the neutron diffusion is factorized into two functions; the shape function $S(z)$ is shown in Figure 4a and amplitude function $S(t)$ of the spallation neutron source could be calculated by:

$$S = \frac{\eta_p}{e} I_p \tag{4}$$

where η_p is the number of spallation neutrons released per proton, e is the electron charge, I_p is the intensity of the proton beam that can be derived by the following formula [30]:

$$I_p = \frac{P_f \nu}{E_f} \frac{e}{\eta_p} \frac{1 - k_{eff}}{k_{eff}} \tag{5}$$

where P_f is the total thermal power of the subcritical core, E_f is the averaged energy released per fission, k_{eff} is the effective multiplication factor, which is an important concept in reactor physics. When neutron disappearance does not equal neutron regeneration, k_{eff}

is introduced to the steady state diffusion equation for criticality calculation, and the subcriticality $1 - k_{eff}$ could be obtained, which means the distance from a criticality. After an external source is added into the subcritical core, the neutron population is perfectly balanced; thus, k_{eff} should be eliminated in the ADS steady state calculation.

2.2.3. Macroscopic Cross Section Generation

Taking into account the Doppler effect and the coolant feedback effect, the parameters of macroscopic cross sections (D, Σ_a and $\nu\Sigma_f$) are mainly related to fuel temperature T_f and coolant density ρ_c in Equation (1). The calculation of macroscopic cross sections is performed using a lattice physics code at different temperature points [26]. Then the values of these parameters $D(T_f, \rho_c)$, $\Sigma_a(T_f, \rho_c)$ and $\nu\Sigma_f(T_f, \rho_c)$ could be obtained by a linear interpolation method. Finally, the one-dimensional equivalent parameters are obtained from flux volume weighting in three-dimensional space:

$$M_i = \frac{\int\limits_{V_i} M(\boldsymbol{r})\phi(\boldsymbol{r})dV}{\int\limits_{V_i} \phi(\boldsymbol{r})dV} \tag{6}$$

where M_i is the average value of the macroscopic cross-section (D, Σ_a and $\nu\Sigma_f$) in axial node i, $\boldsymbol{r}$ is the position vector in three-dimensional space, $\boldsymbol{r}$ is the volume of axial node i.

2.3. Thermal-Hydraulics Model

During the normal operation of the reactor, the fission energy produced by the nuclear fuel is transferred from the fuel pellet to the cladding, and then transferred from the cladding to the coolant. In this work, a single channel model is performed for the thermal-hydraulics calculation, which includes the heat conduction in fuel element and the heat transfer from cladding to coolant.

2.3.1. Heat Conduction in Fuel Elements

In order to obtain the spatial distribution of temperatures of fuel and cladding, the fuel element is divided into K nodes in the axial direction and L nodes in the radial direction, as shown in Figure 5. Since the thickness and thermal resistance of cladding are much smaller than those of the fuel pellet, the cladding is only divided into three nodes in the radial direction to obtain its inner surface and outer surface temperatures. Axial heat conduction is ignored because of prevailing radius to length ratios and axial symmetry [31]. Therefore, the heat conduction equation for the fuel pellet in the axial node i could be written as:

$$\rho_f^i C_f^i \frac{\partial T_f^i(r,t)}{\partial t} = \frac{1}{r}\frac{\partial}{\partial r}\left(rk_f^i \frac{\partial T_f^i(r,t)}{\partial r}\right) + q_v^i \tag{7}$$

where ρ_f^i and C_f^i denote the density and specific heat of the fuel pellet in the axial node i, respectively, T_f^i and k_f^i denote the temperature and heat conductivity of the fuel pellet in the axial node i, respectively, q_v^i is the volumetric heat rate.

Ignoring the heat generated in the cladding, we obtain the heat conduction equation for the cladding in the axial node i as:

$$\rho_{cl}^i C_{cl}^i \frac{\partial T_{cl}^i(r,t)}{\partial t} = \frac{1}{r}\frac{\partial}{\partial r}\left(rk_{cl}^i \frac{\partial T_{cl}^i(r,t)}{\partial r}\right) \tag{8}$$

where ρ_{cl}^i and C_{cl}^i denote the density and specific heat of the cladding in the axial node i, respectively, T_{cl}^i and k_{cl}^i denote the temperature and heat conductivity of the cladding.
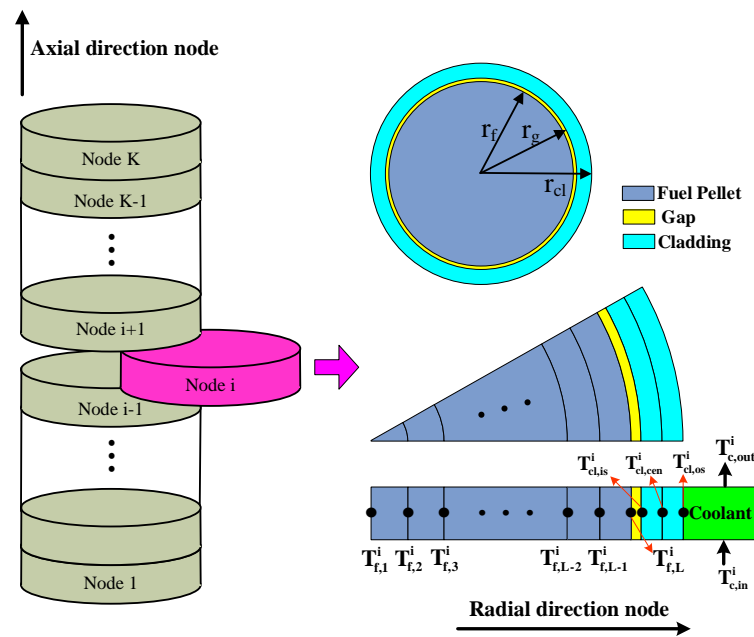
Figure 5. Node division in a fuel element.

2.3.2. Heat Transfer to Coolant

The heat transfer from cladding to coolant in the *i*th node along the reactor axis direction can be described by the basic mass and energy conservation equations as:

$$\rho_c^i V_c^i C_c^i \frac{dT_c^i}{dt} = h_{cl,c}^i A_{cl,c}^i \left(T_{cl}^i \Big|_{r=r_{cl}} - T_c^i \right) - G_c^i C_c^i \left(T_{c,out}^i - T_{c,in}^i \right) \tag{9}$$

where ρ_c^i, V_c^i, C_c^i and T_c^i denote the density, volume, specific heat and temperature of coolant in the axial node *i*, respectively, $h_{cl,c}^i$ denotes the heat transfer coefficient between cladding and coolant, $A_{cl,c}^i$ is the heat transfer area between cladding and coolant, G_c^i denote the mass flow rate of coolant, and $T_{c,in}^i$ and $T_{c,out}^i$ denote coolant inlet and outlet temperatures, respectively.

In the design of fast spectrum reactors, heavy liquid metals such as lead or LBE are usually adopted as the coolant materials for high heat transfer coefficient and large heat capacity. The fuel assembly in the core is usually composed of triangular rod bundles, and thus the Ushakov correlation is used to analyze the heat transfer correlation between the heavy liquid metal coolant and the cladding [32]. The heat transfer coefficient between cladding and coolant is calculated by:

$$h_{cl,c} = \frac{k_c}{D_c} N_u \tag{10}$$

where k_c is the heat conductivity of the coolant, D_c is the hydraulic equivalent diameter; the Nusselt number N_u in the rod bundles is as follows:

$$N_u = 7.55 \frac{p}{d} - 20 \left(\frac{p}{d} \right)^{-13} + \frac{3.67}{90(p/d)^2} Pe^{(0.56+0.19p/d)} \tag{11}$$

where p/d is the ratio of the pitch of fuel pins to its diameter, Pe is the Peclet number. It is valid for $1.2 < p/d < 2.0$, and $1 < Pe < 4000$.

The package of thermophysical properties of materials was developed to insert into the thermal hydraulic model based on the experimental data and empirical correlation [33,34]. The correlations of the thermophysical properties of coolant, cladding, and fuel are presented in Table 1.

Table 1. Thermophysical Properties of Fuel, Cladding, and Coolant.

Thermophysical Parameters	Correlation
Fuel density (kg·m^{-3})	$11080[1 + 2.04 \times 10^{-5}(T - 273) + 8.7 \times 10^{-9}(T - 273)^2]^{-1}$
Fuel thermal conductivity (W·m^{-1}·K^{-1})	$(0.042 + 2.71 \times 10^{-4}T)^{-1} + 6.9 \times 10^{-11}T^3$
UO$_2$ specific heat (J·kg^{-1}·K^{-1})	$81.825 + 0.78695T - 1.1552 \times 10^{-3}T^2 + 9.9037 \times 10^{-7}T^3 - 5.1982 \times 10^{-10}T^4 + 1.5241 \times 10^{-13}T^5 - 1.7906 \times 10^{-17}T^6$
PuO$_2$ specific heat (J·kg^{-1}·K^{-1})	$-4.9236 \times 10^6 T^{-2} + 240.89 + 0.32556T - 3.5398 \times 10^{-4}T^2 + 1.512 \times 10^{-7}T^3 - 1.9707 \times 10^{-11}T^4$
Fuel specific heat (J·kg^{-1}·K^{-1})	$0.7944C_{UO_2} + 0.2056C_{PuO_2}$
Cladding density (kg·m^{-3})	$7785[1 - 3(-3.0942 \times 10^{-3} + 1.1928 \times 10^{-5}T - 6.7979 \times 10^{-9}T^2 + 7.9606 \times 10^{-12}T^3 - 2.546 \times 10^{-15}T^4)]$
Cladding thermal conductivity (W·m^{-1}·K^{-1})	$21.712 + 0.011T - 9.5483 \times 10^{-6}T^2 + 3.627 \times 10^{-9}T^3$
Cladding specific heat (J·kg^{-1}·K^{-1})	$432.8 + 0.7038T - 2.2113 \times 10^{-3}T^2 + 5.316 \times 10^{-6}T^3 - 3.105 \times 10^{-9}T^4$
Coolant density (kg·m^{-3})	$11112 - 1.375T$
Coolant thermal conductivity (W·m^{-1}·K^{-1})	$3.35 + 1.59 \times 10^{-2}T - 1.95 \times 10^{-6}T^2$
Coolant specific heat (J·kg^{-1}·K^{-1})	$164 - 4.06 \times 10^{-2}T + 1.33 \times 10^{-5}T^2$

2.3.3. Heat Exchanger Model

The primary coolant flows out of the core and enters the heat exchanger through the ascending channel. The primary coolant then flows down to the lower plenum after its heat is transferred to the organic diathermic fluid on the secondary side. The schematic diagram of the primary circuit is shown in Figure 6.
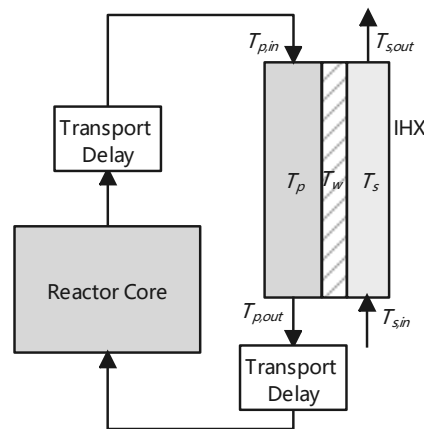
Figure 6. Schematic diagram of primary circuit.

The heat transfer models of primary coolant, tube wall and secondary coolant are as follows:

$$V_p \rho_p C_p \frac{dT_p}{dt} = G_p C_p (T_{p,in} - T_{p,out}) - h_{p,w} A_p (T_p - T_w) \tag{12}$$

$$V_w \rho_w C_w \frac{dT_w}{dt} = h_{p,w} A_p (T_p - T_w) - h_{s,w} A_s (T_w - T_s) \tag{13}$$

$$V_s \rho_s C_s \frac{dT_s}{dt} = h_{s,w} A_s (T_w - T_s) - G_s C_s (T_{s,out} - T_{s,in}) \tag{14}$$

where $h_{p,w}$ is the heat transfer coefficient between primary coolant and tube wall, $h_{s,w}$ denotes the heat transfer coefficient between tube wall and secondary coolant.

The ARTAP code has been verified by comparing its predictions for both steady-state and transient cases of the OECD/NEA benchmark [12]. The benchmark summarizes a comparative analysis of ten different codes. Three cited codes for the comparison are: TRAC-MOD, SAS4ADS and EXCURS-M, as they represent the range of data scatter in the published results of the benchmark report. The results indicate that ARTAP is accurate and efficient when applied for the safety analysis of the LBE-cooled ADS and CNES [26].

3. Results and Discussions

The Italian 80 MW LBE-cooled reactor was chosen as the LBE-cooled ADS or equivalent critical system to investigate the safety characteristics in this work. The arrangement of assemblies and horizontal view of one-sixth of the ADS core and the CNES core are shown in Figure 7. The ADS core is divided into several regions, as shown in Figure 7a. The inner region consists of 120 hexagonal fuel assemblies, and the dummy assemblies in the outer region mainly contain LBE which is taken as the reflector. The central channel is designed to introduce proton beam into the spallation neutron target. The outside of the core region is filled with LBE coolant, which serves as axial reflector and radial reflector. The CNES core has a similar configuration without the spallation target, as shown in Figure 7b, in which 19 additional fuel assemblies are added in the central channel to bring the reactor to critical state without external neutron source. In both the ADS and CNES systems, each fuel assembly includes 90 triangle-distributed fuel rods made of MOX pellet (PuO_2/UO_2 with 23% Pu) in a stainless steel cladding. The main technical design parameters of these two reactors are listed in Table 2. Three typical accidents are carried out to study the difference of transient behaviors between ADS and CNES, which include reactivity insertion, loss of flow, and loss of heat sink.

(a) **ADS assembly arrangement**　　　　　　　　　(b) **CNES assembly arrangement**
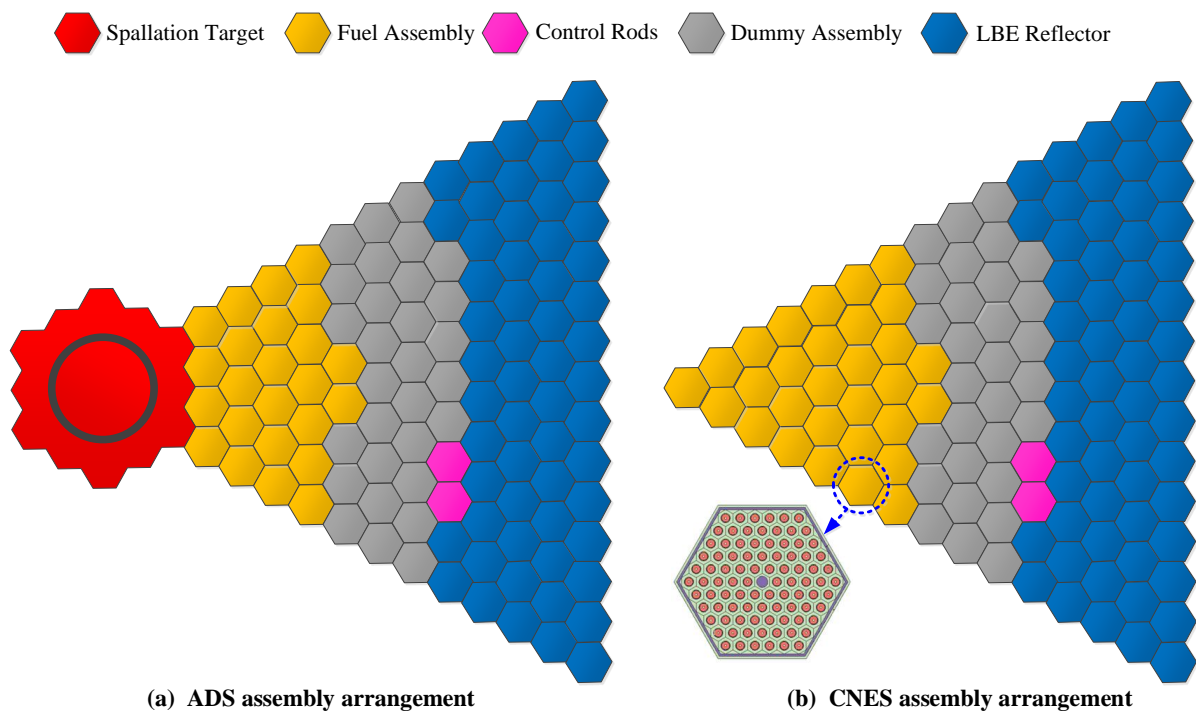
Figure 7. Horizontal view of assembly arrangement for one-sixth of the ADS core and the CNES core.

Table 2. Main design parameters of the ADS and CNES reactors.

Parameters	ADS	CNES
Proton energy (MeV)	600	-
Intensity of proton beam (mA)	2.5	-
Effective multiplication factor k_{eff}	0.97	1.04
Total thermal power (MW)	80	
Fuel element height (m)	0.9	
Fuel pellet outer diameter (m)	7.14×10^{-3}	
Cladding inner diameter (m)	7.37×10^{-3}	
Cladding outer diameter (m)	8.5×10^{-3}	
Coolant flow area (m^2)	9.89×10^{-5}	
Pin pitch (m)	1.341×10^{-2}	
Core inlet temperature (K)	573	
Core outlet temperature (K)	673	

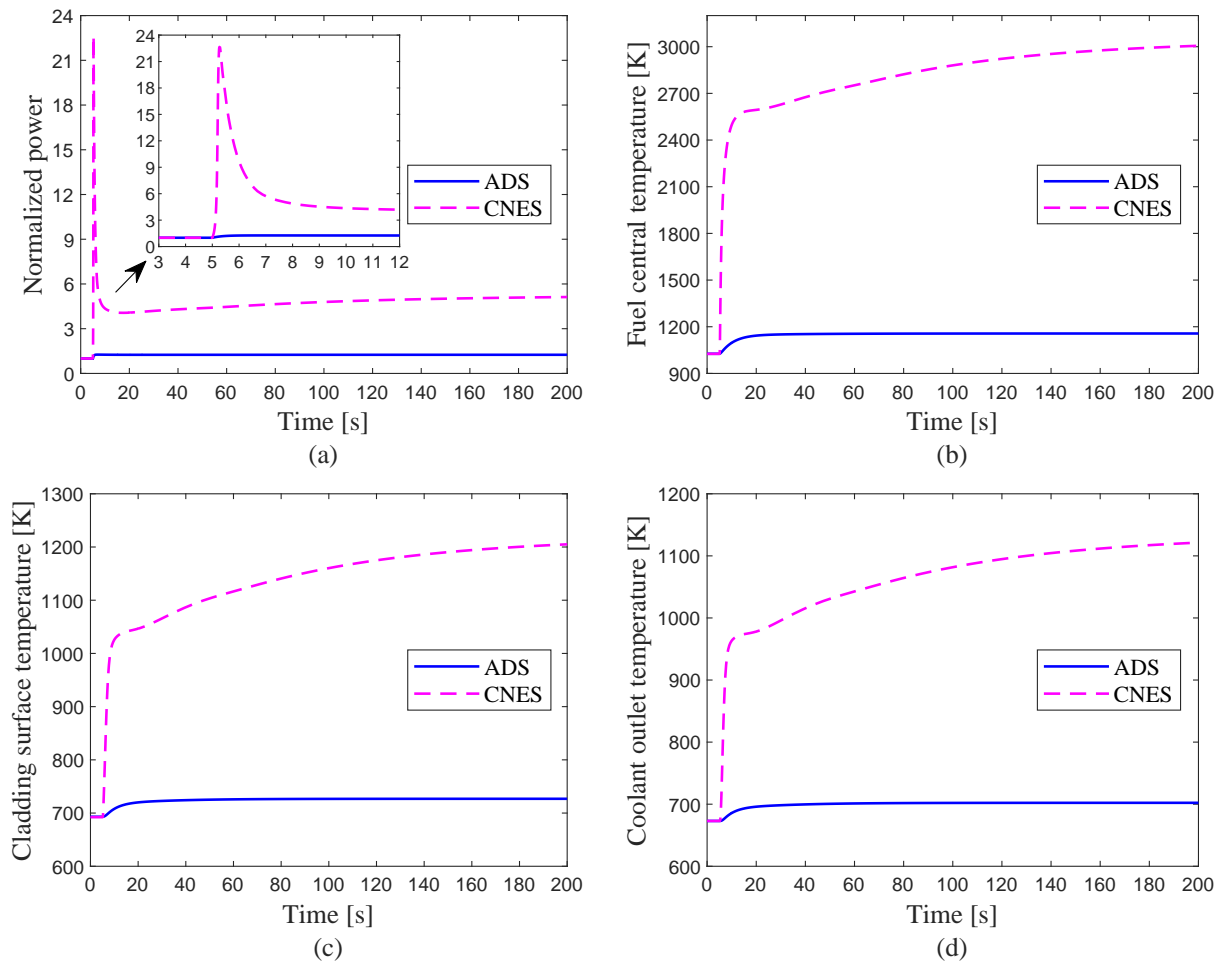*3.1. Reactivity Insertion Accident*

During the operation of nuclear reactors, due to the failure of mechanical devices or the misoperation of personnel, the control rods are accidentally ejected and then positive reactivity is introduced, causing the reactor power to deviate from normal operating conditions. The introduction of instantaneous positive reactivity may lead to a sharp increase in the temperatures of the fuel pellet and the cladding, and even a rupture in the fuel element. In this paper, the reactivity insertion is realized by the control rod, and the approach is to adjust the absorption cross-section $\Sigma_{a,rod}(z)$ of the control rod in Equations (1) and (3), where z is the insertion depth of the control rod. Reactivity insertion accidents of 700 pcm (about 2$) for ADS and CNES are simulated, and the comparative safety analysis of these two reactors is carried out. In addition, the accident simulation is not only performed in the case of unprotected transient, but also in the case of protected transient, i.e., transient with interruption of accelerator beam for ADS and with insertion of shutdown rod for CNES. The transient behaviors of the reactor power and the temperatures of the fuel, cladding, and coolant are investigated during the accident sequences.

3.1.1. Unprotected Reactivity Insertion

The Transient responses of ADS and CNES for unprotected reactivity insertion of 700 pcm are shown in Figure 8. It can be seen from Figure 8a that the ADS power only increases by about 25% after 700 pcm reactivity is introduced into the core, and then the power decreases slightly due to the negative reactivity introduced by the Doppler feedback effect and the coolant temperature feedback effect, and finally reaches a new equilibrium value. Meanwhile, the temperatures of the fuel center, cladding surface, and coolant outlet also ascend with the power increase and then gradually stabilize to a new equilibrium point. This is principally because the ADS reactor is a subcritical core driven by an external neutron source, in which the k_{eff} is far from the critical point and the neutron multiplication capacity is weak after the core is inserted positive reactivity. Therefore, the power only rises to 1.25 times the steady-state value, and the maximum temperatures of fuel pellet and cladding are far below the safety limit under the unprotected reactivity insertion accident. The results show that the ADS has good inherent safety in the event of reactivity insertion accident, and its margin of criticality safety is large.

The simulation results also show that the the CNES power rose sharply to nearly 22 times the steady-state value under unprotected reactivity insertion accident. At the same time, the negative feedback effect of reactivity caused by the substantial increase of the fuel and coolant temperatures suppresses the continuous increase of the power, and finally the power drops to about five times the steady-state value. However, the peak temperature of the fuel center reaches 3012 K, which is close to the melting point. The peak temperature of the cladding surface is 1205 K, which means it has exceeded the damage limit. This is mainly because CNES

enters a prompt supercritical state after 700 pcm (about 2 $) reactivity is instantly introduced into the critical core, and the power grows exponentially. The comparison results show the power and the temperatures of fuel pellet, cladding, and coolant of the CNES core are much higher than those of the ADS core during the reactivity insertion accident, which means ADS has a better safety advantage than CNES.
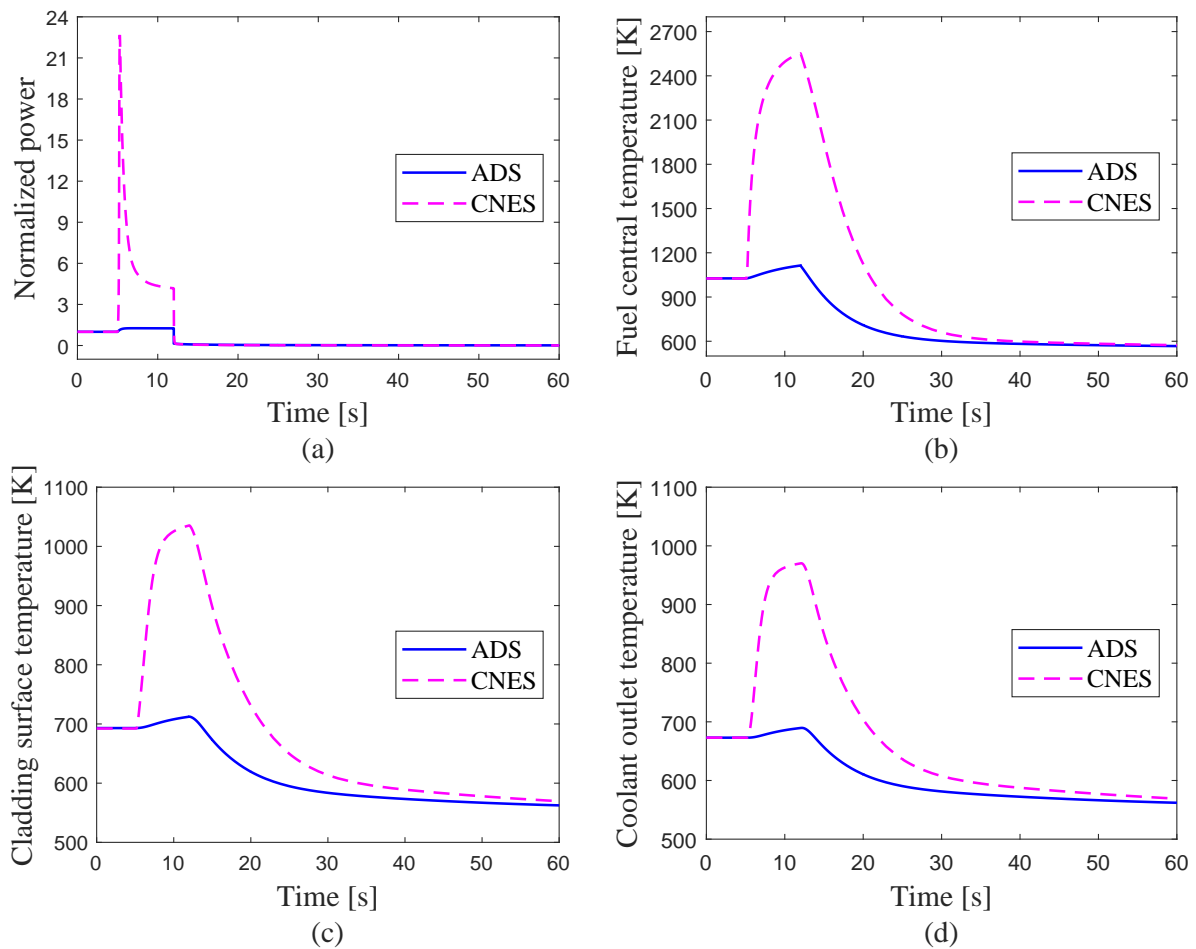

Figure 8. Transient responses of unprotected reactivity insertion of 700 pcm between the ADS core and the CNES core.

3.1.2. Protected Reactivity Insertion

After a serious accident occurs, the shutdown protection system is activated so that the reactor can quickly return to a safe state. For the CNES reactor, the safety control rod is quickly inserted to shut down the reactor. This process takes about 1~2 s. The ADS reactor could be shut down by cutting off the proton beam to interrupt the external neutron source in the subcritical core. The time required from detecting the accident information to cutting off the beam is only about 1 ms, which is faster than the activation of the mechanical device of shutdown rod.

The transient responses of protected reactivity insertion for ADS and CNES are shown in Figure 9, in which the positive reactivity is inserted at 5 s and then the shutdown protection system is activated at 12 s. For the ADS reactor, it can be seen that the power and the temperatures of fuel, cladding, and coolant sharply decrease to the safety level after the proton accelerator is closed. After introducing 700 pcm reactivity for the CNES reactor, the prompt supercritical accident occurs, and then the power and the fuel temperature rise sharply to very high values. With the rapid insertion of the safety control rod, the power declines to the shutdown level, and the peak temperatures of the fuel center and the cladding surface are 2552 K and 1035 K, respectively. It can be seen from Figure 9c that

the cladding still has a short-term rapture failure risk in the CNES reactor during this transient state.

Figure 9. Transient responses of protected reactivity insertion of 700 pcm between the ADS core and the CNES core.

3.2. Loss of Flow Accident

The influence of the pump trip on the mass flow rate was studied for loss of flow accident in the EBR-II fast reactor [35]. In this work, the loss of flow accidents of ADS and CNES are simulated with ARTAP, in which the coolant mass flow in the core drops from 100% to 10% due to primary pump coastdown. Both unprotected and protected cases are considered.

3.2.1. Unprotected Loss of Flow

Figure 10 shows the transient responses of ADS and CNES for unprotected loss of flow due to primary pump coastdown. The mass flow rate of the reactor core drops rapidly after the primary coolant pump trips, which causes the heat produced by fission reaction in the fuel not to be able to be taken out in time, and the cladding temperature rises rapidly. As shown in Figure 10c, the maximum cladding temperature in the ADS core reaches 1439 K, which means it has exceeded the damage limit. For one thing, the power drop is small due to the deep subcriticality of the ADS core and low sensitivity to negative reactivity feedback, which is from 100% full power to 90% level. Furthermore, the loss of flow rate prevents the heat transferral from the pellet to the coolant, so the temperature of the cladding rises to a very high value. Due to the negative reactivity introduced by the Doppler effect and the coolant temperature effect, the reactor power of CNES quickly decreases from 100% to 41%, and the cladding temperature rises to the peak point and then gradually decreases. The peak temperature of the cladding in the CNES core is only 1005 K,

which is lower than the breakage limit. Results of comparison show that the inherent safety characteristics of the CNES core are better than those of the ADS core under loss of flow accident, and the protection system of ADS should be quickly activated to achieve an emergency shutdown after the accident occurs.
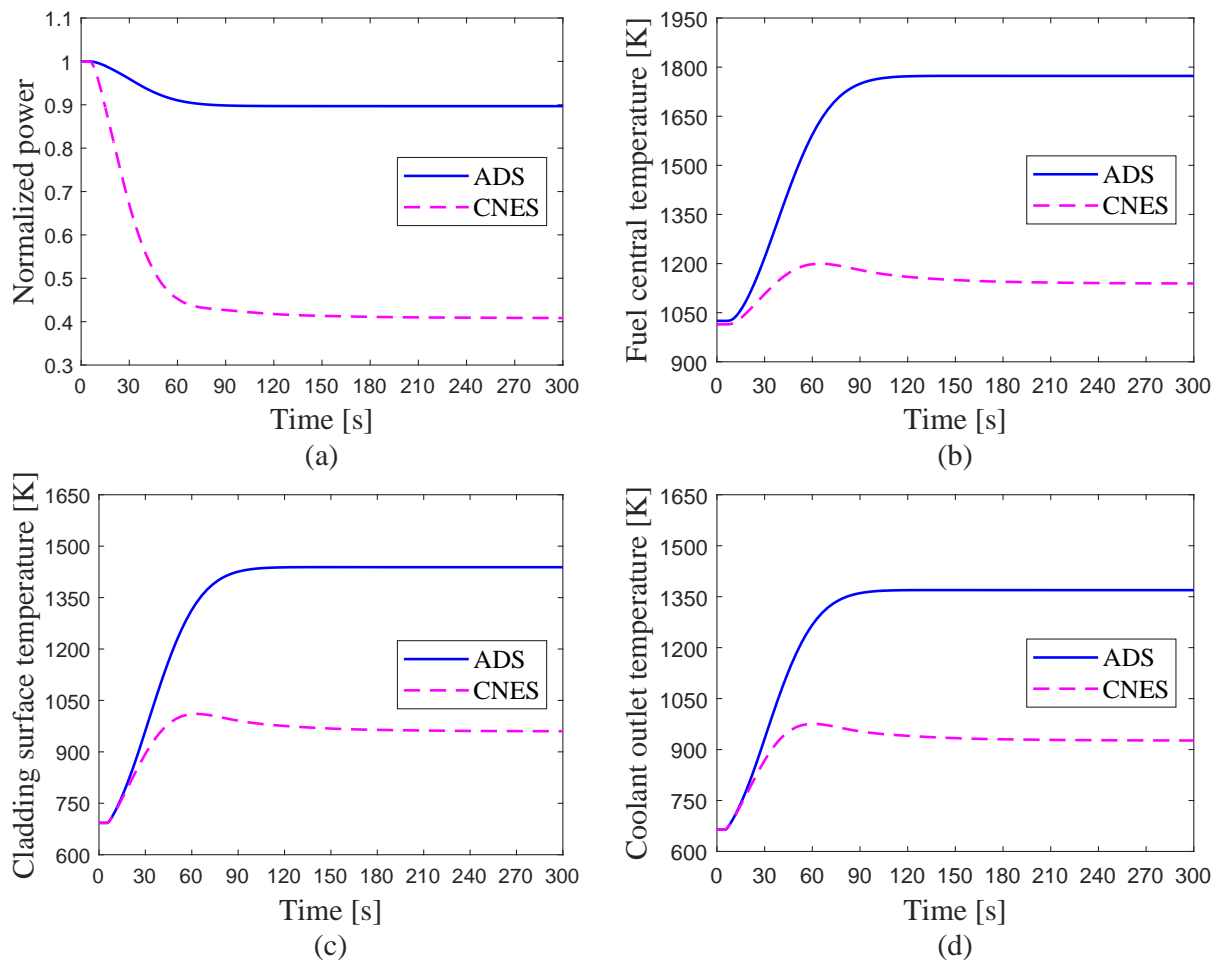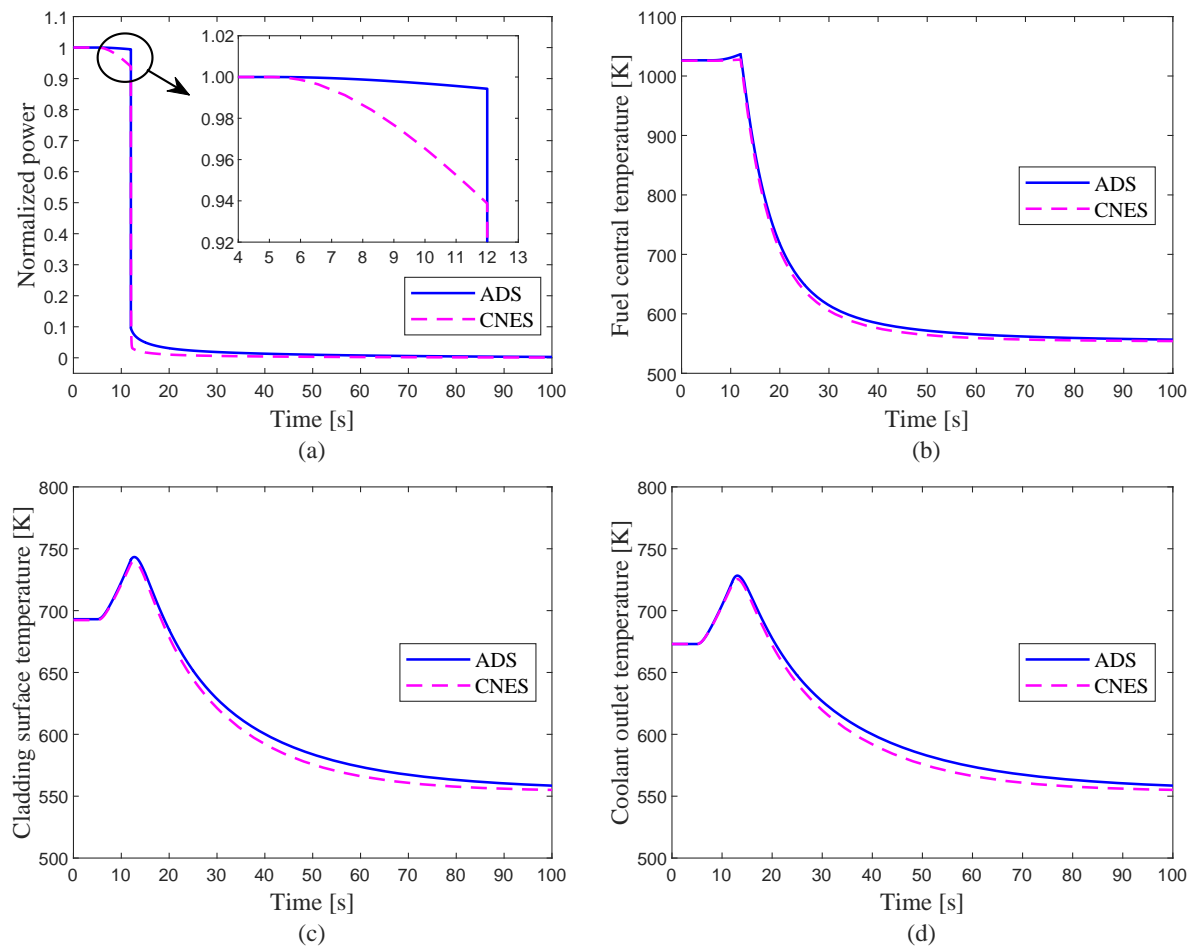

Figure 10. Transient responses of unprotected loss of flow between the ADS core and the CNES core.

3.2.2. Protected Loss of Flow

The calculation results of the protected loss of flow are presented in Figure 11, where the primary pump trips at 5 s, and the shutdown signal occurs at 12 s. It can be seen that the reactor power and the fuel temperature of both ADS and CNES drop rapidly and then reach the shutdown level after the protection system is activated. As shown in Figure 11a, the reactor power of CNES declines faster than that of ADS. During this process, the maximum temperatures of the fuel center and the cladding surface in the ADS and CNES reactors are lower than the security limit. These simulation results indicate that the CNES system could ensure reactor shutdown by inserting safety control rod. It also implies that ADS could quickly restore to safety by cutting off the proton beam under loss of flow accident.
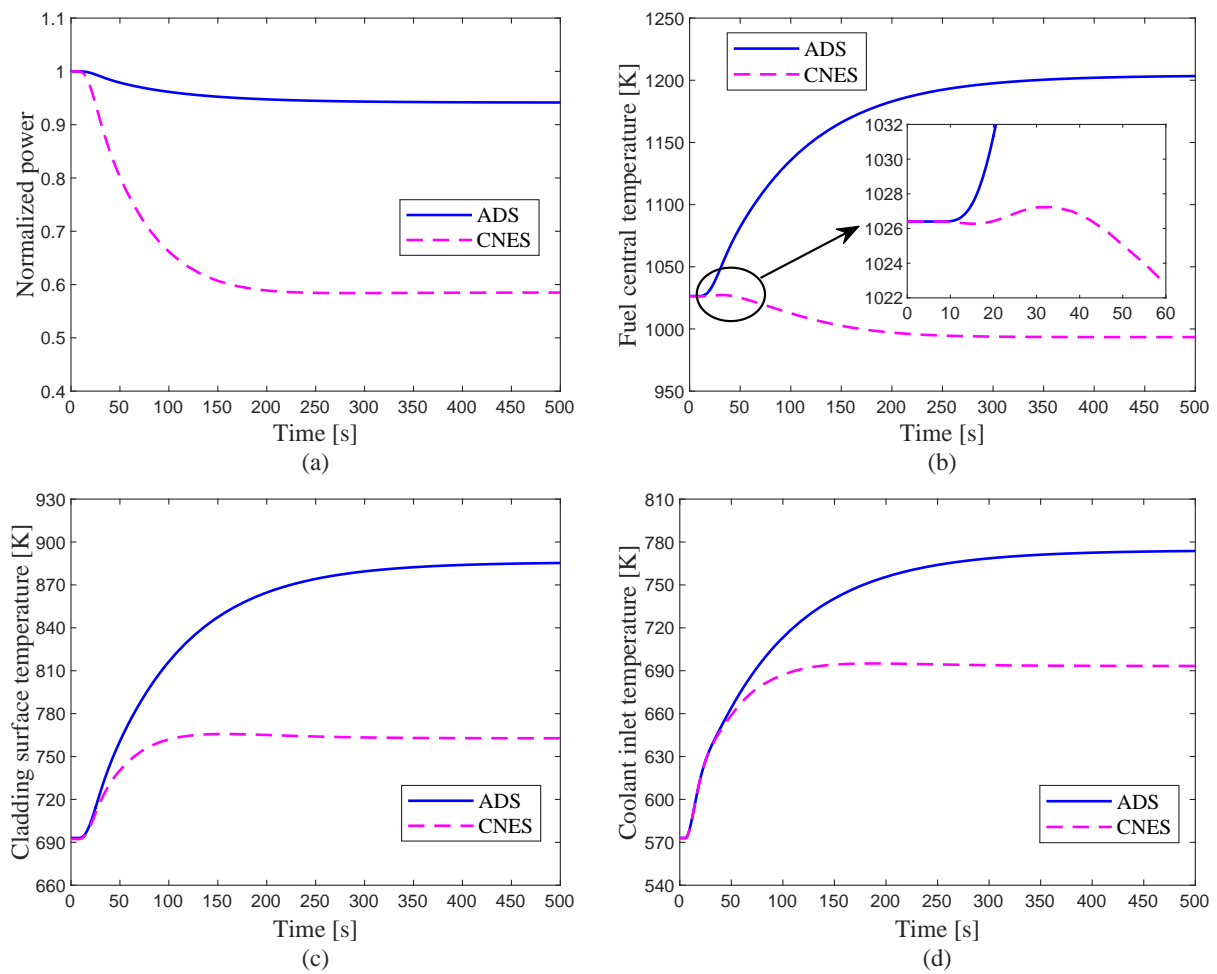
Figure 11. Transient responses of protected loss of flow between the ADS core and the CNES core.

3.3. Loss of Heat Sink Accident

Corresponding to the primary circuit system, the secondary circuit system is a heat sink of the core during the normal operation of nuclear reactors. When the cooling system of the secondary circuit fails, such as all the secondary circuit pumps trip, insufficient cooling capacity of the core results in a heat sink accident [36]. During the process of heat sink accident, all of the circuit pumps in the secondary loop fail, which causes a mass flow of the entire secondary circuit to drop from 100% to 8% within 20 s. Both unprotected and protected cases are examined in this work.
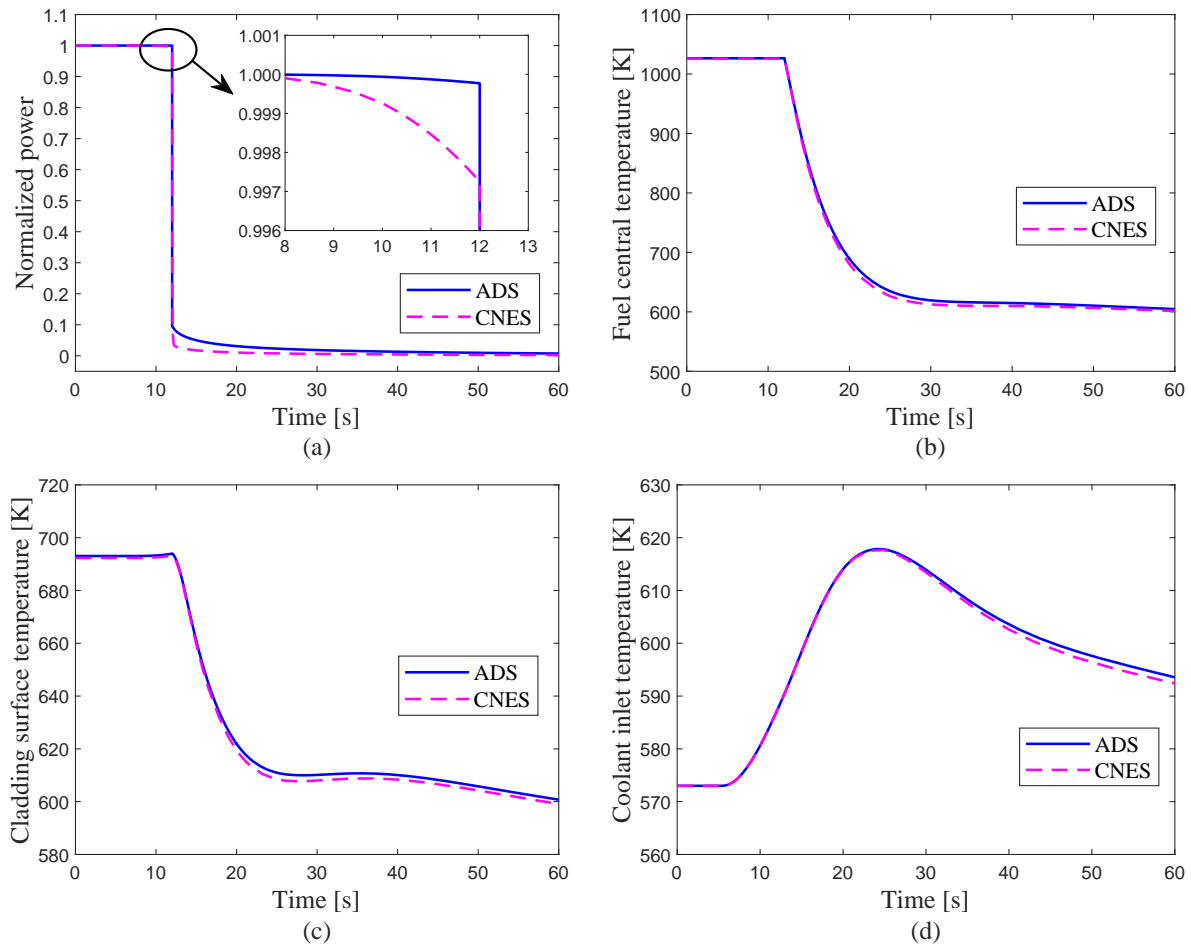
3.3.1. Unprotected Loss of Heat Sink

Transient responses of the ADS core and the CNES core for unprotected loss of heat sink due to all secondary pumps trip are shown in Figure 12. Because the mass flow rate of the secondary side in the heat exchanger drops rapidly after the loss of heat sink accident, the heat of the primary circuit loop cannot be removed in time. It can be seen from Figure 12d that the coolant inlet temperatures of both the ADS core and the CNES core rise rapidly. The power drops due to the negative feedback effect of reactivity, in which the reduction of the CNES power is much larger than that of the ADS power, thus the fuel central temperature of CNES rises slightly and then declines with the decrease of the power. During the loss of heat sink accident, the peak temperatures of the cladding surface in the ADS and CNES reactors are lower than the safety limit.

Figure 12. Transient responses of unprotected loss of heat sink between the ADS core and the CNES core.

3.3.2. Protected Loss of Heat Sink

The simulation results of ADS and CNES for the protected loss of heat sink are shown in Figure 13, where all secondary pumps stop at 5 s, and the shutdown signal occurs at 12 s. As the secondary circuit pumps all stop running, the mass flow rate of the secondary side in the heat exchanger (IHX) drops rapidly, and the outlet temperature of the primary side in the IHX rises, which means that the coolant inlet temperature of the core increases. With the rapid decrease of the reactor power due to the activation of the shutdown protection system, the temperatures of the fuel center and cladding surface also drop rapidly, and then the coolant inlet temperature gradually declines as well. These simulation results indicate that both the ADS and CNES systems have the inherent safety characteristics to ensure reactor a shutdown against loss of heat sink accident.

Figure 13. Transient responses of protected loss of heat sink between the ADS core and the CNES core.

4. Conclusions

In the present study, a developed computational code named ARTAP is used to analyze and compare the safety characteristics between the LBE-cooled ADS and CNES. The developed code consists of a space–time neutron diffusion equation with a spallation neutron source model and a thermal-hydraulics model with a package of thermophysical properties, which could be used for calculations of both the LBE-cooled ADS and the LBE-cooled CNES. In order to investigate differences of the safety characteristics of these two reactors, three typical accidents are carried out, including reactivity insertion, loss of flow, and loss of heat sink. In addition, the accident simulations are not only performed in the case of unprotected transient, but also in the case of protected transient, i.e., transient with interruption of accelerator beam for ADS and with insertion of shutdown rod for CNES. The transient behaviors of the reactor power and the temperatures of the fuel, cladding, and coolant are investigated during the accident sequences.

The comparison results show the power and the temperatures of fuel pellet, cladding, and coolant of the CNES core are much higher than those of the ADS core during the reactivity insertion accident, which means ADS has a better safety advantage than CNES. However, due to the deep subcriticality of the ADS core and its low sensitivity to negative reactivity feedback, the simulation results indicate that the inherent safety characteristics of the CNES core are better than those of the ADS core under loss of flow accident, and the protection system of ADS would be quickly activated to achieve an emergency shutdown after the accident occurs. For the loss of heat sink, it is found that the peak temperatures of the cladding in the ADS and CNES reactors are lower than the safety limit, which mean these two reactors have good safety performance against loss of heat sink accident.

Abbreviations

The following abbreviations are used in this manuscript:

ADS	Accelerator Driven Subcritical System
CNES	Critical Nuclear Energy System
LBE	Lead-Bismuth Eutectic
MOX	Mixed Oxide Fuel

References

1. Maschek, W.; Chen, X.; Delage, F.; Fernandez-Carretero, A.; Haas, D.; Boccaccini, C.M.; Rineiski, A.; Smith, P.; Sobolev, V.; Thetford, R.; et al. Accelerator driven systems for transmutation: Fuel development, design and safety. *Prog. Nucl. Energy* **2008**, *50*, 333–340. [CrossRef]
2. Kumar, V.V.; Katovsky, K. A Comprehensive Review of Developments of Accelerator Driven Subcritical Systems and Future Requirements. In Proceedings of the IEEE 2020 21st International Scientific Conference on Electric Power Engineering (EPE), Prague, Czech Republic, 19–21 October 2020; pp. 1–6.
3. Cinotti, L.; Giraud, B.; Abderrahim, H.A. The experimental accelerator driven system (XADS) designs in the EURATOM 5th framework programme. *J. Nucl. Mater.* **2004**, *335*, 148–155. [CrossRef]
4. Van Tuyle, G.; Hill, D.; Beller, D.; Bishop, W.; Cotton, T.; Finck, P.; Halsey, W.; Herezeg, J.; Herring, J.; Lancaster, D.; et al. A roadmap for developing ATW technology: System scenarios & integration. *Prog. Nucl. Energy* **2001**, *38*, 3–23.
5. Hill, R.; Khalil, H. *Physics Studies for Sodium Cooled ATW Blanket*; Technical Report; Argonne National Laboratory: Lemont, IL , USA, 2001.
6. Yang, W.S.; Khalil, H.S. Blanket design studies of a lead-bismuth eutectic-cooled accelerator transmutation of waste system. *Nucl. Technol.* **2001**, *135*, 162–182. [CrossRef]
7. Sugawara, T.; Takei, H.; Iwamoto, H.; Oizumi, A.; Nishihara, K.; Tsujimoto, K. Research and development activities for accelerator-driven system in JAEA. *Prog. Nucl. Energy* **2018**, *106*, 27–33. [CrossRef]
8. Park, W.S.; Shin, U.; Han, S.J.; Song, T.Y.; Choi, B.H.; Park, C.K. HYPER (Hybrid Power Extraction Reactor): A system for clean nuclear energy. *Nucl. Eng. Des.* **2000**, *199*, 155–165. [CrossRef]
9. Wu, Y. Design and R&D progress of China lead-based reactor for ADS research facility. *Engineering* **2016**, *2*, 124–131.
10. Huang, Y.L.; Liu, L.B.; Jiang, T.C.; Wang, R.X.; Zhang, S.X.; Guo, H.; Li, C.L.; Liu, S.H.; Lin, Z.Q.; Tan, T.; et al. 650 MHz elliptical superconducting RF cavities for CiADS Project. *Nucl. Instrum. Methods Phys. Res. Sect. A Accel. Spectrometers Detect. Assoc. Equip.* **2021**, *988*, 164906. [CrossRef]
11. Yan, X.; Yang, L.; Zhang, X.; Zhan, W. Concept of an accelerator-driven advanced nuclear energy system. *Energies* **2017**, *10*, 944. [CrossRef]
12. D'Angelo, A.; Arien, B.; Sobolev, V.; Van den Eynde, G.; Gabrielli, F. Benchmark on beam interruptions in an accelerator-driven system, Final Report on Phase I Calculations. In *Organisation for Economic Co-Operation and Development*; Nuclear Energy Agency: Paris, France, 2003; Volume 17, 28p, ISBN 92-64-02138-8.
13. Chen, X.; Suzuki, T.; Rineiski, A.; Wiegner, E.; Maschek, W.; Flad, M. Unprotected transients in a small scale accelerator driven system. In Proceedings of the International Topical Meeting on Nuclear Applications of Accelerator Technology (AccApp'03), San Diego, CA, USA, 1–5 June 2003; pp. 1–5.

14. Suzuki, T.; Chen, X.N.; Rineiski, A.; Maschek, W. Transient analyses for accelerator driven system PDS-XADS using the extended SIMMER-III code. *Nucl. Eng. Des.* **2005**, *235*, 2594–2611. [CrossRef]

15. Wang, G.; Gu, Z.; Wang, Z.; Jin, M. Verification of Neutronics and Thermal-hydraulics Coupled Simulation Program NTC by the PDS-XADS transient simulation. *Prog. Nucl. Energy* **2015**, *85*, 659–667. [CrossRef]

16. Wang, Z.; Wang, G.; Gu, Z.; Jin, M.; Wu, Y. Benchmark of neutronics and thermal-hydraulics coupled simulation program NTC on beam interruptions in XADS. *Ann. Nucl. Energy* **2015**, *77*, 172–175. [CrossRef]

17. Lu, T.; Shan, J.; Gou, J.; Zhang, B.; Zhang, B.; Ge, L.; Yuan, Y.; Yang, Z. Preliminary safety analysis on loss of flow accidents and external source transients for LBE cooled ADSR core. *Prog. Nucl. Energy* **2016**, *88*, 134–146. [CrossRef]

18. Schikorr, W. Assessments of the kinetic and dynamic transient behavior of sub-critical systems (ADS) in comparison to critical reactor systems. *Nucl. Eng. Des.* **2001**, *210*, 95–123. [CrossRef]

19. Mikityuk, K.; Coddington, P.; Pelloni, S.; Bubelis, E.; Chawla, R. Comparative transient analysis of critical and subcritical 80-MW Pb-Bi eutectic-cooled reactor systems. *Nucl. Technol.* **2007**, *157*, 18–36. [CrossRef]

20. Wang, G.; Gu, Z.; Wang, Z.; Jin, M. Comparison of transient analysis of LBE-cooled fast reactor and ADS under loss of heat sink accident. *Ann. Nucl. Energy* **2015**, *85*, 494–500. [CrossRef]

21. Eriksson, M.; Cahalan, J.E.; Yang, W.S. On the performance of point kinetics for the analysis of accelerator-driven systems. *Nucl. Sci. Eng.* **2005**, *149*, 298–311. [CrossRef]

22. Rineiski, A.; Maschek, W. Kinetics models for safety studies of accelerator driven systems. *Ann. Nucl. Energy* **2005**, *32*, 1348–1365. [CrossRef]

23. Shampine, L.F.; Reichelt, M.W.; Kierzenka, J.A. Solving index-1 DAEs in MATLAB and Simulink. *SIAM Rev.* **1999**, *41*, 538–552. [CrossRef]

24. Savović, S.; Djordjevich, A.; Peter, W.T.; Nikezić, D. Explicit finite difference solution of the diffusion equation describing the flow of radon through soil. *Appl. Radiat. Isot.* **2011**, *69*, 237–240. [CrossRef]

25. Cammi, A.; Luzzi, L.; Porta, A.A.; Ricotti, M.E. Modelling and control strategy of the Italian LBE-XADS. *Prog. Nucl. Energy* **2006**, *48*, 578–589. [CrossRef]

26. Luo, R.; Wang, P.; Wei, X.; Revankar, S.T.; Zhao, F. Development of Neutronics and Thermal-Hydraulics Coupled Code for Accelerator Driven Subcritical Systems. In Proceedings of the 2018 26th International Conference on Nuclear Engineering, London, UK, 22–26 July 2018; American Society of Mechanical Engineers Digital Collection: New York, NY, USA, 2018.

27. Song, H.; Luo, R.; Wan, J.; Li, S.; Zhao, F. Development of a novel 1D coupled neutronics/thermal-hydraulics code and its verification on PWR rod ejection accident benchmark. *Prog. Nucl. Energy* **2016**, *92*, 197–210. [CrossRef]

28. Duderstadt, J.J.; Hamilton, L.J. *Nuclear Reactor Analysis*; JohnWiley & Sons Inc.: New York, NY, USA, 1976.

29. Pelowitz, D.B. *MCNPXTM User'S Manual*; Los Alamos National Laboratory: Los Alamos, NM, USA, 2005.

30. Zhou, S.; Wu, H.; Cao, L.; Zheng, Y.; Huang, K.; He, M.; Li, X. LAVENDER: A steady-state core analysis code for design studies of accelerator driven subcritical reactors. *Nucl. Eng. Des.* **2014**, *278*, 434–444. [CrossRef]

31. Wulff, W.; Cheng, H.; Mallen, A. *Analytical Modeling Techniques for Efficient Heat Transfer Simulation in Nuclear Power Plant Transients*; Technical Report; Brookhaven National Laboratory: Upton, NY, USA, 1985.

32. Pfrang, W.; Struwe, D. *Assessment of Correlations for Heat Transfer to the Coolant for Heavy Liquid Metal Cooled Core Designs*; Forschungszentrum Karlsruhe GmbH: Karlsruhe, BW, Germany, 2007; Volume 7352.

33. D'Angelo, A.; Arien, B.; Sobolev, V.; Van den Eynde, G.; Gabrielli, F. Benchmark on beam interruptions in an accelerator-driven system, Final Report on Phase II Calculations. In *Organisation for Economic Co-Operation and Development*; Nuclear Energy Agency: Paris, France, 2004; Volume 79.

34. Sobolev, V. *Database of Thermophysical Properties of Liquid Metal Coolants for Gen-IV*; Scientific Rep. the Belgian Nuclear Research Centre: Antwerp, Belgium, 2011.

35. Messick, N.; Betten, P.; Booty, W.; Christensen, L.; Fryer, R.; Mohr, D.; Planchon, H.; Radtke, W. Modification of EBR-II plant to conduct loss-of-flow-without-scram tests. *Nucl. Eng. Des.* **1987**, *101*, 13–23. [CrossRef]

36. Feldman, E.; Mohr, D.; Chang, L.; Planchon, H.; Dean, E.; Betten, P. EBR-II unprotected loss-of-heat-sink predictions and preliminary test results. *Nucl. Eng. Des.* **1987**, *101*, 57–66. [CrossRef]